ECCM-2001

European Conference on
Computational Mechanics

June 26-29, 2001
Cracow, Poland

INFLUENCE OF THE ELEMENT TYPE ON THE ACCURACY OF CREEP–DAMAGE PREDICTIONS IN THIN-WALLED STRUCTURES

Konstantin Naumenko, Holm Altenbach and Chunxiao Huang

Department of Engineering Sciences
Matrin-Luther-University Halle-Wittenberg, Germany
e–mail: holm.altenbach@iw.uni-halle.de

Vyacheslav Burlayenko

Department of Applied Mathematics
National Technical University KhPI, Kharkov, Ukraine
e–mail: burlayenko@kpi.kharkov.ua

Key words: Creep Damage, Shells, Finite Element Analysis

Abstract. *Based on the continuum creep-damage mechanics and the finite element analysis the long-term strength in thin-walled structures is estimated using the solid and the shell type finite elements available in ANSYS code. For this purpose the material model with a scalar damage parameter is incorporated into the ANSYS code with the help of a user defined material subroutine. The results based on the first order shear deformation beam equations are compared with the results of the finite element plane stress simulations. It is demonstrated that the shear correction factor and the distribution function of the transverse shear stress have to be modified within time-step calculations. For a rectangular plate in bending finite element analysis is performed based on the shell and the solid type finite elements. The differences in the edge-zone stress redistributions in the shell and the solid type models as well as the influence of boundary layer solutions on the long-term predictions are illustrated.*

---

1 Introduction

Continuum damage mechanics (CDM) has become an efficient tool for the analysis of long-term behaviour in structures at elevated temperatures [1]. Based on a suitable constitutive model with internal state variables characterising hardening and damage processes the deformation, the stress and the damage fields in a structure can be predicted by solving nonlinear initial-boundary value problems. Applying the finite element method two possibilities are usually available for the analysis of thin-walled structures. The first one is the application of three-dimensional equations and solid type finite elements. The second one is the use of the models of beams, plates and shells, which are based on the through-the-thickness approximations of three-dimensional displacement and stress fields and corresponding finite element implementations. The solid based concept can be considered as general, particularly in CDM analysis of structures with stress concentrations or weldments [2]. However, in the case of thin-walled structures great effort is necessary for numerical treatment of the three-dimensional equations and the solution may lead to conditioning problems. With the progress in the material science and continuum mechanics various new material models are proposed including physically motivated state variables and considering stress state dependences. On the other hand the available models of beams, plates and shells are based on simplified cross-section assumptions and have been originally developed within the theory of linear elasticity (e.g. [3, 4]). A number of investigations show that the classical Kirchhoff-Love and first order shear deformation shell theories can accurately predict the creep deformation and creep buckling of shells considering material models of primary and secondary creep [5, 6, 7]. The introduction of damage requires to take into account non-classical effects in the material behaviour, e.g. different tertiary creep rates by tension and compression or anisotropic behaviour induced by damage. As demonstrated in [8] the effect of different damage rates in tension and compression induces non-symmetrical through-the-thickness damage distributions in a plate in bending, whereas the analysis has been based on the first order shear deformation theory. In [9, 10] the creep-damage analysis for a thin-walled pipe bend is performed using the shell and the solid type finite elements. It is shown that the shell and the solid models lead to different life-time estimations if the damage evolution induces a non-symmetrical through-the-thickness behaviour. Furthermore, different edge-zone stress redistributions may result as a consequence of the creep-damage process.

The aim of this paper is to discuss the numerical creep-damage predictions in simple structures: a thin-walled beam and a rectangular plate in bending. Particularly we examine the first order shear deformation shell theory, which is mostly used in the finite element codes. Firstly we derive the beam equations considering the effect of creep deformation and damage evolution demonstrating the possibilities and limitations of the cross-section assumptions. Based on the numerical study of a beam we demonstrate that the shear correction factor and the distribution function of the transverse shear stress have to be modified within time-step calculations. Secondly we perform the finite element analysis for a rectangular plate in bending based on the shell and the solid type finite elements. The differences in the boundary layer solutions based on the shell and the solid type models as well as their influence on the long-term predictions will be discussed in detail. Finally we discuss the requirements for the through-the-thickness approximations in refined models for beams, plates and shells.

2 Material Behaviour and Consequences for Structural Mechanics Models

Creep behaviour of polycrystalline metals and alloys is a complex phenomenon accompanied by different microstructural changes. It is known from material science that for moderate stresses (below the yield limit) and elevated temperatures above $0.4T_m$ with T_m as the melting point, the steady state creep process is controlled by the climb plus glide dislocation mechanism [11, 12]. The strain rate can be predicted using the power law stress function. For multi-axial stress states the deviatoric stress components and the von Mises equivalent stress are responsible for the deformation process. In addition to irreversible strains, material deterioration processes occur and lead to accelerated creep in the tertiary stage and to the final fracture. For polycrystalline materials the tertiary creep is accompanied by nucleation and growth of cavities on grain boundaries. The initially existing micro-defects have negligible influence on the strain rate. As their number and size increase with time, they weaken the material providing the decrease in the load-bearing cross section. The nucleation kinetics can be related to the local grain boundary deformation as well as to the stress state characterised by the first positive principal stress (maximum tensile stress) and the von Mises equivalent stress [13]. The coalescence of cavities lead to propagation of oriented microcracks and to the final fracture. Further the damage evolution induces anisotropic creep response. The cavities and microcracks nucleate on grain boundaries having different orientations. The significant influence of the damage anisotropy can be observed on the last stage before the creep rupture.

Let us introduce the conventional creep-damage material model of Kachanov-Rabotnov-Hayhurst [14]

$$\dot{\varepsilon}_{ij}^{cr} = \frac{3}{2}a\left(\frac{\sigma_{vM}}{1-\omega}\right)^n \frac{s_{ij}}{\sigma_{vM}}, \quad \dot{\omega} = b\frac{[\alpha\sigma_I + (1-\alpha)\sigma_{vM}]^k}{(1-\omega)^l} \tag{1}$$

In this notation $\dot{\varepsilon}_{ij}^{cr}$ are the components of the creep strain rate tensor, s_{ij} are the components of the stress deviator, σ_{vM} is the von Mises stress, σ_I is the maximum positive principal stress and ω is the damage parameter. α is a weighting coefficient allowing to consider the influence of principal damage mechanisms(σ_I-controlled or σ_{vM}-controlled). The material constants are taken for the 316 stainless steel at 650°C from [15]: $a = 2.13 \cdot 10^{-13}$ MPa^{-n}/h, $b = 9 \cdot 10^{-10}$ MPa^{-k}/h, $n = 3.5$, $k = 2.8$, $l = 2.8$, $\alpha = 1$. The isotropic elasticity without influence of damage has been assumed with $E = 1.44 \cdot 10^5$ MPa as Young's modulus and $\nu = 0.314$ as Poisson's ratio.

According to the discussed mechanisms the primary and secondary creep rates are dominantly controlled by the von Mises stress. The accelerated creep is additionally influenced by the kind of the stress state. For example, different tertiary creep rates and fracture times can be obtained from creep tests performed under uniaxial tension with the stress σ and under torsion with the shear stress $\tau = \sigma/\sqrt{3}$ [16]. Fig. 1a) shows creep curves for tensile, compressive and shearing stresses simulated by the constitutive model (1) with the introduced material constants. The corresponding stress values provide the same value of the von Mises equivalent stress. It is obvious that the tertiary creep rate is significantly dependent on the kind of loading. Fig. 1b) presents creep curves calculated by the combined action of the normal and shear stresses. It is seen that even the small superposed shear stress can significantly influence the axial strain response and decrease the fracture time. On the other hand, the change of the sign of the normal stress influences both the normal and shear creep responses. The stress states with combined normal tensile (compressive) stress and small shear stress are typical for the transversely loaded beams, plates and shells. Fig. 2 shows creep responses under biaxial and triaxial stress states. It can be

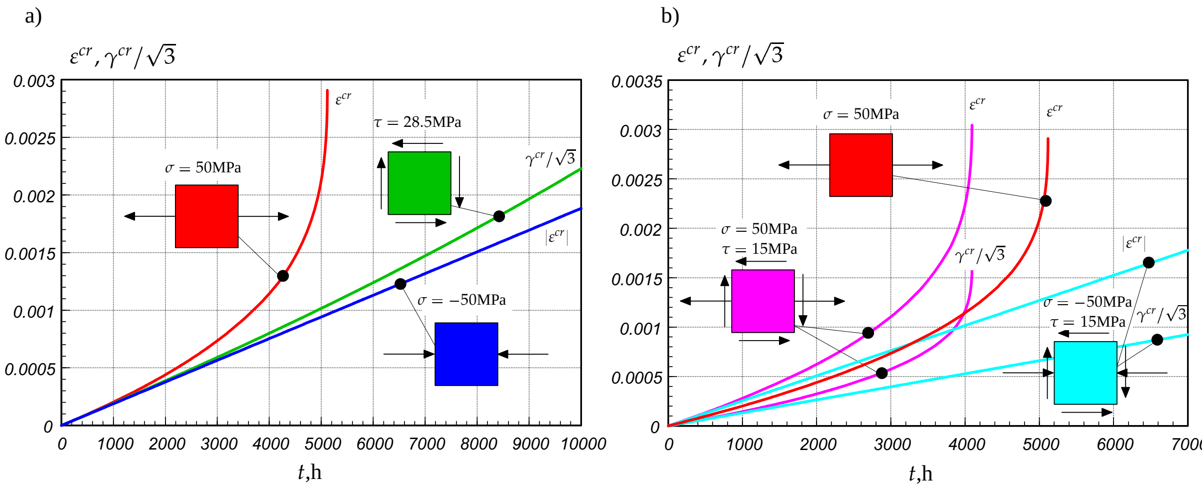

Figure 1: Creep responses for various stress states computed using equations (1): (a) responses by tension, torsion and compression; (b) responses by combined tension (compression) and torsion

observed that even a small superposition of the third principal stress significantly reduces the von Mises creep strain rate. For the triaxial stress state with equal principal stresses the model (1) yields the zero equivalent creep strain rate. The fracture time remains unchanged for all stress states presented in Fig. 2 since the damage evolution is controlled by the maximum principal stress. The experimental results on creep-damage under triaxial stress state are discussed in [17].

Based on the creep damage material response let us discuss the requirements regarding the through-the-thickness assumptions for modelling of thin-walled structures. Firstly, since even the small shear stress can significantly influence the material response, the transverse shear stress and the resulting transverse shear strain cannot be neglected. Thus at least the first order shear deformation model has to be used for the creep damage analysis. Secondly, the dependence of the creep response on the sign of the normal stress can lead to the non-symmetrical thickness distributions of the displacement, the strain and the stress fields. This has to be considered by specifying the through-the-thickness approximations for displacements or stresses. Finally, the transverse normal stresses which are usually neglected in the theory of elastic shells and plates should be considered since they can significantly influence the creep responses.

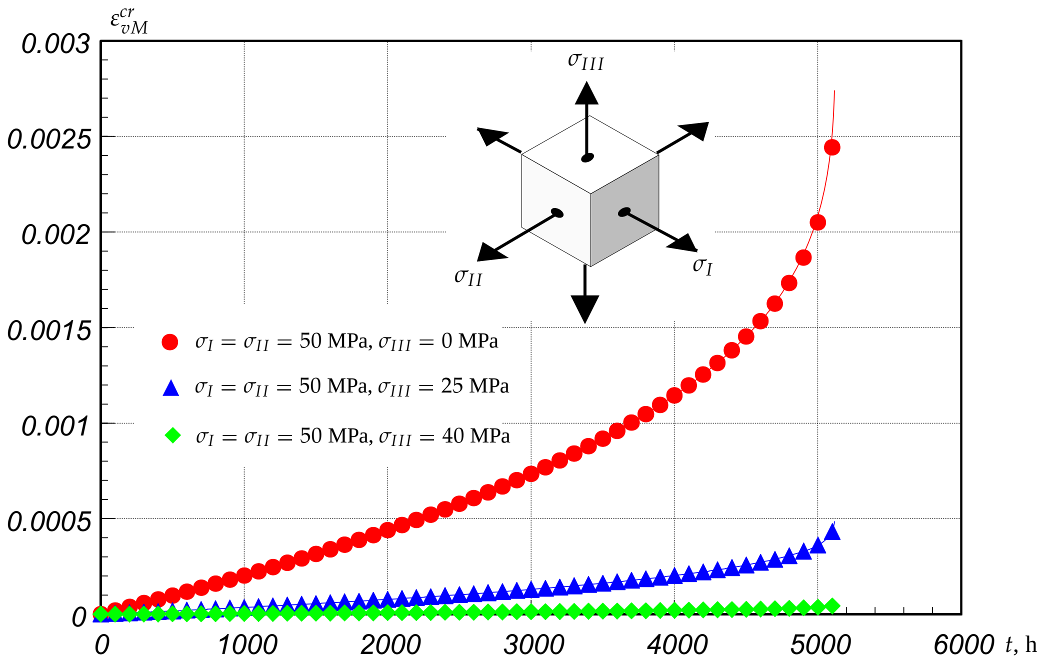

Figure 2: Von Mises creep strain vs. time for different stress states

3 Observations on Beam Equations

In what follows we discuss the assumptions of the first order shear deformation theory in detail and introduce the beam equations. The following simplified derivations will provide conclusions regarding cross-section assumptions in connection with the effect of the creep damage. Let us consider a beam with a rectangular cross-section, Fig. 3. Considering the beam as a plane stress

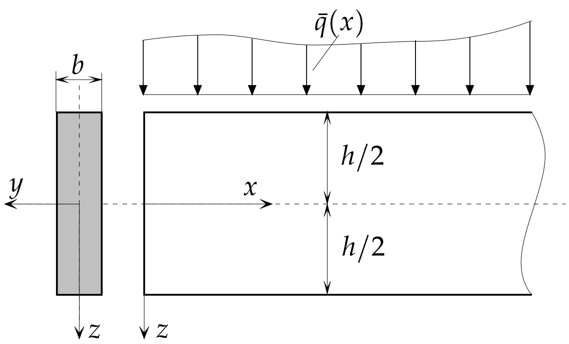

Figure 3: Straight beam with a rectangular cross section in Cartesian coordinates

problem the principle of virtual displacements yields

$$-\delta W_i = \frac{bh}{2} \int_0^l \int_{-1}^1 (\sigma_x \delta\varepsilon_x + \tau_{xz}\delta\gamma_{xz} + \sigma_z \delta\varepsilon_z) d\zeta dx = \int_0^l \bar{q}(x)\delta w(x, -h/2) dx = \delta W_a \quad (2)$$

Here l denotes the beam length, $\sigma_x, \sigma_y, \tau_{xz}$ and $\varepsilon_x, \varepsilon_y, \gamma_{xz}$ are the components of the stress and strain tensors, respectively, w is the beam deflection and $\zeta = 2z/h$ is the thickness coordinate. Here and in the following derivations we use the abbreviations

$$\frac{\partial}{\partial x}(\ldots) \equiv (\ldots)_{,x}, \quad \frac{\partial}{\partial z}(\ldots) \equiv (\ldots)_{,z},$$
$$\frac{d}{dx}(\ldots) \equiv (\ldots)', \quad \frac{d}{d\zeta}(\ldots) \equiv (\ldots)^{\bullet}, \quad \frac{d}{dt}(\ldots) \equiv (\dot{\ldots})$$

For the sake of simplicity we assume the absence of tractions on the edges $x = 0$ and $x = l$. Specifying the through-the-thickness approximations of axial displacement u and deflection w, various engineering displacement based beam theories can be obtained, e.g. [18]. For example, a refined displacement based beam model can be obtained with

$$u(x,\zeta) = u_0(x) + \varphi(x)\frac{h}{2}\zeta + u_1(x)\Phi(\zeta), \quad w(x,\zeta) = w_0(x) + w_1(x)\Omega(\zeta), \tag{3}$$

where u_0 and w_0 are the displacements of the beam centreline, φ is the cross section rotation, $\Phi(\zeta)$ and $\Omega(\zeta)$ are distribution functions, which should be specified, and $u_1(x)$ and $w_1(x)$ are unknown functions of the x–coordinate.

Another possibility is the use of stress based approximations, for example, following from the elasticity solution of the Bernoulli-Euler beam equations

$$\sigma_x = \frac{6M(x)}{bh^2}\zeta, \quad \tau_{xz} = \frac{3Q(x)}{2bh}\left(1 - \zeta^2\right), \quad \sigma_z = \frac{3\bar{q}(x)}{4b}\left(-\frac{2}{3} + \zeta - \frac{1}{3}\zeta^3\right), \tag{4}$$

where Q and M are the shear force and the bending moment, respectively. Applying the stress approximations E. Reissner derived the elasticity plate equations by means of the mixed variational equation [19]. The displacement approximations (3) neglecting the terms $u_1\Phi$ and $w_1\Omega$ or the stress approximations (4) lead to a first order shear deformation beam theory. By generalisation the corresponding models of plates and shells can be obtained. The stress approximations (4) are not suitable for creep problems because even for the steady state creep solution of a beam the normal stress σ_x is non-linearly distributed along the thickness coordinate [20].

Let us derive the first order shear deformation beam equations without assumptions for the stress σ_x. The transverse shear and the transverse normal stresses can be approximated as follows

$$\tau_{xz} = \frac{2Q(x)}{bh}\frac{\psi^{\bullet}(\zeta)}{\psi_0}, \quad \sigma_z = \frac{\bar{q}(x)}{b}\frac{\psi(\zeta) - \psi(1)}{\psi_0}, \quad \psi_0 = \psi(1) - \psi(-1) \tag{5}$$

$\psi(\zeta)$ is a given function satisfying the boundary conditions $\psi^{\bullet}(\pm 1) = 0$. The variation of the work of the internal forces W_i in Eq. (2) can be written as

$$-\delta W_i = \frac{bh}{2}\int_0^l \int_{-1}^1 \delta(\tau_{xz}\gamma_{xz} + \sigma_z\varepsilon_z) - \underline{(\gamma_{xz}\delta\tau_{xz} + \varepsilon_z\delta\sigma_z - \sigma_x\delta\varepsilon_x)}d\zeta dx \tag{6}$$

With the approximations (5) and the linear strain-displacement equations $\varepsilon_x = u_{,x}$, $\varepsilon_z = w_{,z}$ and $\gamma_{xz} = u_{,z} + w_{,x}$ we obtain

$$\frac{bh}{2}\int_0^l \int_{-1}^1 \delta(\tau_{xz}\gamma_{xz} + \sigma_z\varepsilon_z)d\zeta dx = \int_0^l \left[\delta(Q\tilde{w}' - Q\tilde{u}) + \bar{q}\delta w(x,-1) - \bar{q}\delta\tilde{w}\right] dx \tag{7}$$

with

$$\tilde{w}(x) = \frac{1}{\psi_0}\int_{-1}^1 w(x,\zeta)\psi^{\bullet}(\zeta)d\zeta, \qquad \tilde{u}(x) = \frac{2}{h}\frac{1}{\psi_0}\int_{-1}^1 u(x,\zeta)\psi^{\bullet\bullet}(\zeta)d\zeta \tag{8}$$

Let us assume the additive split of the total strain tensor into an elastic and a creep part

$$\varepsilon_{ij} = \varepsilon_{ij}^{el} + \varepsilon_{ij}^{cr},$$

and ε_{ij}^{cr} to be known functions of the coordinates x, ζ for the fixed time variable. Further we will use the linear through-the-thickness approximation of the axial displacement

$$u(x,\zeta) = u_0(x) + \varphi(x)\zeta\frac{h}{2}$$

With these assumptions the underlined term in equation (6) can be transformed into

$$\int_0^l \left[N'\delta u_0 + M'\delta\varphi + \frac{1}{Gbhk}Q\delta Q + \tilde{\gamma}^{cr}\delta Q\right] dx \tag{9}$$

with the shear modulus G and

$$\begin{aligned} N(x) &= \frac{bh}{2}\int_{-1}^1 \sigma_x(x,\zeta)d\zeta, \quad & M(x) &= \frac{bh^2}{4}\int_{-1}^1 \sigma_x(x,\zeta)\zeta d\zeta, \\ \frac{1}{k} &= \frac{2}{\psi_0^2}\int_{-1}^1 \psi^{\bullet 2}(\zeta)d\zeta, & \tilde{\gamma}^{cr}(x) &= \frac{1}{\psi_0}\int_{-1}^1 \gamma_{xz}^{cr}(x,\zeta)\psi^{\bullet}(\zeta)d\zeta \end{aligned} \tag{10}$$

After summing up all terms in Eq. (2) we obtain the following variational equation

$$\int_0^l \left[(Q - M')\delta\varphi - (Q' + \bar{q})\delta\tilde{w} - N'\delta u_0 + \left(\varphi + \tilde{w}' - \frac{1}{Gbhk}Q - \tilde{\gamma}^{cr}\right)\delta Q\right] dx = 0 \tag{11}$$

Assuming the variations of the functions u_0, φ, $\tilde{w}$ and Q to be independent Eq. (11) provides the following ordinary differential equations

$$N' = 0, \quad M' - Q = 0, \quad Q' + \bar{q} = 0, \quad Q = Gbhk(\varphi + \tilde{w}' - \tilde{\gamma}^{cr}) \tag{12}$$

The first three equations are the classical equilibrium conditions of the beam. The last equation is the constitutive equation connecting the shear force and the averaged shear strain. From this equation and with the assumed linear through-the-thickness approximation of the axial displacement we obtain

$$u(x,\zeta) = u_0(x) - \zeta\frac{h}{2}\tilde{w}'(x) + \zeta\frac{h}{2}\frac{Q(x)}{Gbhk} + \zeta\frac{h}{2}\tilde{\gamma}^{cr}(x)$$

The second term is the rotation of the normal to the centreline (Bernoulli's hypothesis), the third term denotes the influence of the shear force in the sense of the Timoshenko theory, and the last term is the contribution of the averaged creep shear strain. The coefficient k and the average of the creep strain $\tilde{\gamma}^{cr}$ are unknown while the function $\psi^\bullet(\zeta)$ is not specified. The parabolic shear stress distribution function according to the solution of the elastic Bernoulli beam $\psi^\bullet(\zeta) = 1 - \zeta^2$ yields the classical shear correction factor $k = 5/6$ for a homogeneous rectangular cross-section.

Let us consider the classical steady state creep solution of a Bernoulli beam [20]. Assuming the Norton-Bailey creep law we obtain

$$\dot{\varepsilon}_x \approx \dot{\varepsilon}_x^{cr} = a\sigma_x^n = -\dot{w}''\zeta\frac{h}{2}$$

The stress σ_x can be expressed as

$$\sigma_x(x,\zeta) = \left(-\frac{\dot{w}''}{a}^{1/n}\right)|\zeta|^{(1/n)-1}\zeta\left(\frac{h}{2}\right)^{1/n} = \frac{M(x)}{\alpha bh^2}|\zeta|^{(1/n)-1}\zeta, \quad \alpha = \frac{n}{2(2n+1)}$$

After inserting this equation into the equilibrium condition

$$\sigma_{x,x} + \frac{2}{h}\tau_{xz,\zeta} = 0 \tag{13}$$

and the integration with respect to the ζ coordinate, the distribution function can be obtained as

$$\psi^\bullet(\zeta) = 1 - \zeta^2|\zeta|^{(1/n)-1} \tag{14}$$

Inserting this function into the first equation (10) we obtain $k_n = (3n+2)/(4n+2)$. Setting $n = 1$ this equation yields the shear correction factor of elastic beam with rectangular cross-section. Since the value of n varies between 3 and 10 for metallic materials we can estimate, for example, if $n = 3; 10$, $k_n = 11/14; 16/21$, respectively. It can be seen that k_n in the case of steady state creep is influenced by the creep exponent. The value of k_n decreases with increasing creep exponent (for $n \to \infty$ we obtain $k_\infty = 3/4$). Because the effect of damage is connected with the increase of the creep strain rate, the decreasing of the shear correction coefficient can be expected if damage evolution is taken into account. In addition, if the damage rate differs for tensile and compressive stresses, the thickness distribution of the transverse shear stress will be non-symmetrical. In this case the function $\psi^\bullet$ cannot be selected a-priori. In [10] the function $\psi^\bullet$

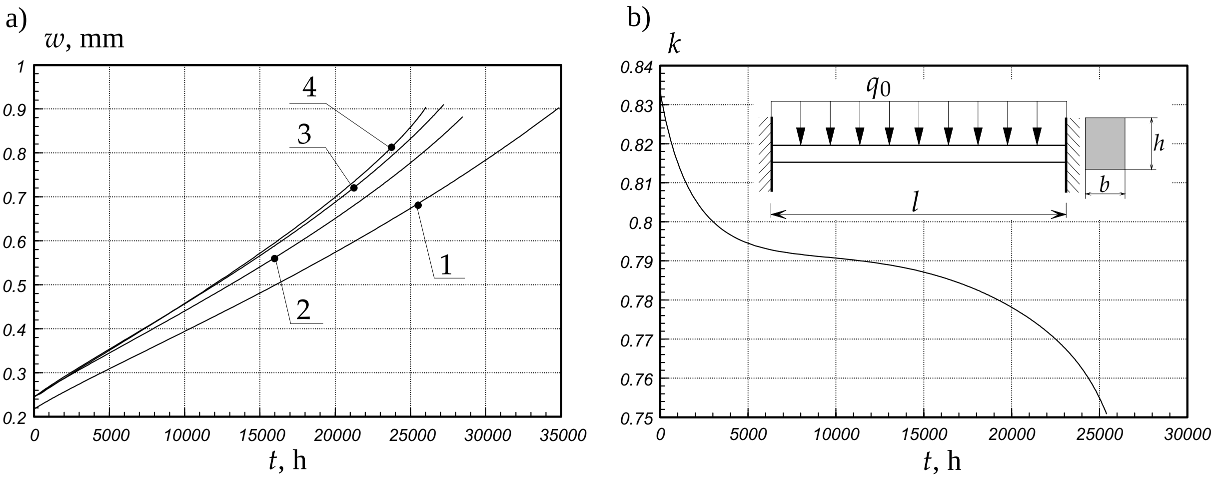

Figure 4: Time dependent solutions of a clamped beam: (a) maximum deflection vs. time; (b) shear correction factor vs. Time, 1 – Bernoulli-Euler beam theory, 2 – first order shear deformation theory with parabolic shear stress distribution, 3 – first order shear deformation theory with modified shear stress, 4 – solution using the ANSYS code with PLANE 42 elements

and the shear correction factor have been estimated for the creep-damage problem of a clamped beam. Fig. 4 presents the simulation results for the uniformly loaded beam with clamped edges. For the calculations we set $l = 1000$ mm, $b = 50$ mm, $h = 100$ mm and $q_0 = 50$ N/mm. The material model (1) with introduced material constants is used. The curve 1 on the Fig. 4a) is the time dependent maximum deflection calculated by use of the Bernoulli-Euler beam theory. The corresponding equations and the numerical procedure are presented in [21]. The curve 2 is obtained using the beam model with the parabolic transverse shear stress according to Eqs (4) and the shear correction coefficient as $5/6$. The curve 3 is the solution based on the equations discussed above with the modified function $\psi^\bullet(\zeta)$. The numerical method which allows to compute the function $\psi^\bullet(\zeta)$ within the time-step schema is presented in [10]. The curve 4 is the ANSYS code finite element solution obtained with plane elements PLANE 42. It is obvious that the Bernoulli-Euler beam theory cannot adequately predict the deflection growth. Further, the first order shear deformation theory underestimates the deflection particularly on the last stage of the creep process. By modification of the transverse shear stress distribution function a better agreement between the elementary beam theory and the plane stress solution is obtained. Fig. 4b) presents the dependence on time of the shear correction factor. With decreasing value of k we can conclude that the influence of the shear correction terms in the discussed equations increases.

The damage evolution in the beam is dominantly controlled by the maximum positive bending stresses. Fig. 5 shows the distribution of the damage parameter at the last step of calculation. Fig. 6a) presents the distribution of the transverse shear stress τ_{xz} obtained by ANSYS code with PLANE 42 elements. It can be observed that near the beam edges where the maximum damage occurs the distribution is non-symmetrical across the thickness direction. Fig. 6b) shows the solution according to the derived beam equations. The transverse shear stress can be calculated

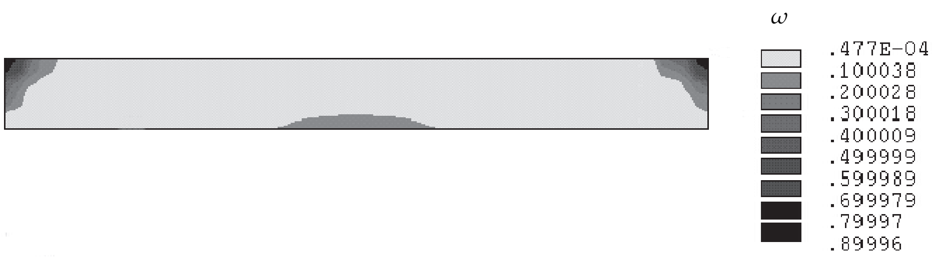

Figure 5: Damage distribution in a beam at last time step

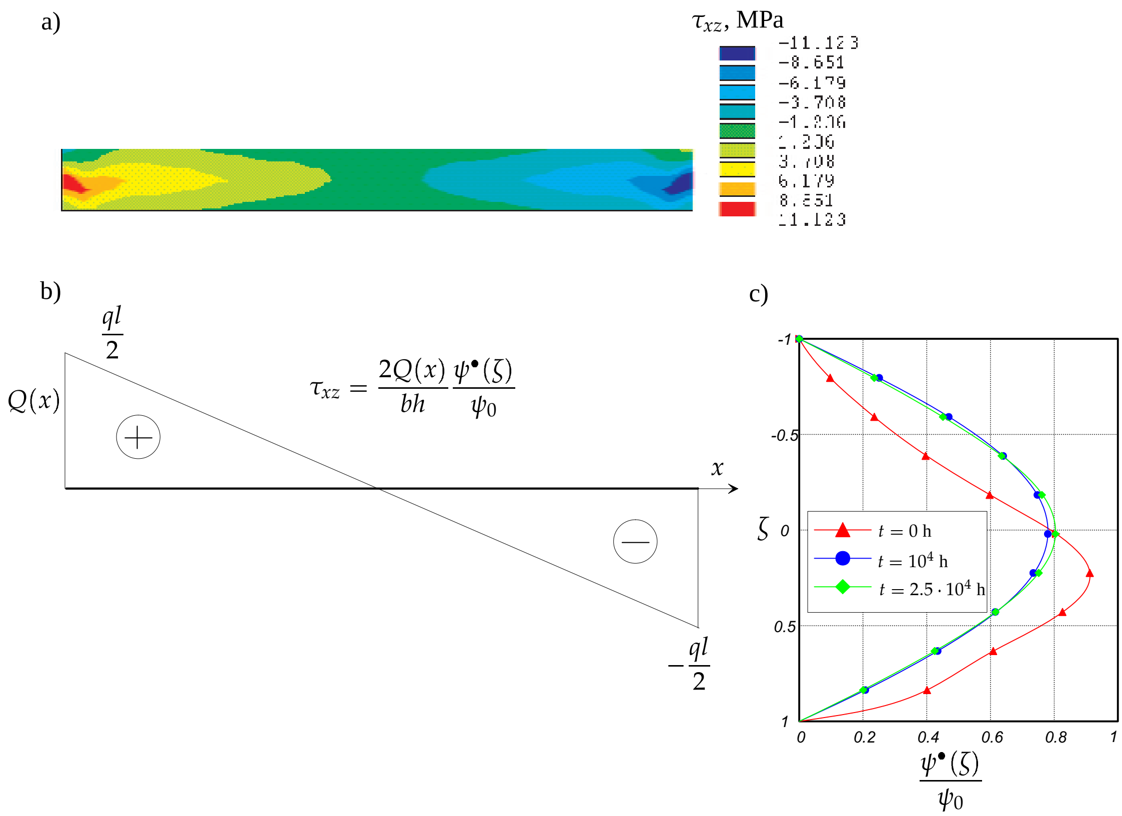

Figure 6: Transverse shear stresses in a beam: (a) τ_{xz} at last time step, solution with PLANE 42 elements; (b) shear force distribution according to the beam equations; (c) function of the transverse shear stress distribution for different time steps

as a product of the shear force and the function of the distribution $\psi^\bullet$ with a constant factor. Since for the considered beam the shear force remains constant during the creep process (it is statically determinate) the time-dependence of the transverse shear stress is determined by the time-dependence of the function $\psi^\bullet$. This function is computed based on the method discussed in [10] and plotted in Fig. 6c) for different time steps.

4 Numerical Analysis of Plate in Bending Based on Solid and Shell Elements

In order to demonstrate the boundary layer effects let us perform a finite element analysis of a rectangular plate in bending. As an example we selected the square plate $l_x = l_y = 1000$ mm, $h = 100$ mm loaded by an uniformly distributed force $q = 2$ N/mm^2, Fig. 7. The edges $x = 0$

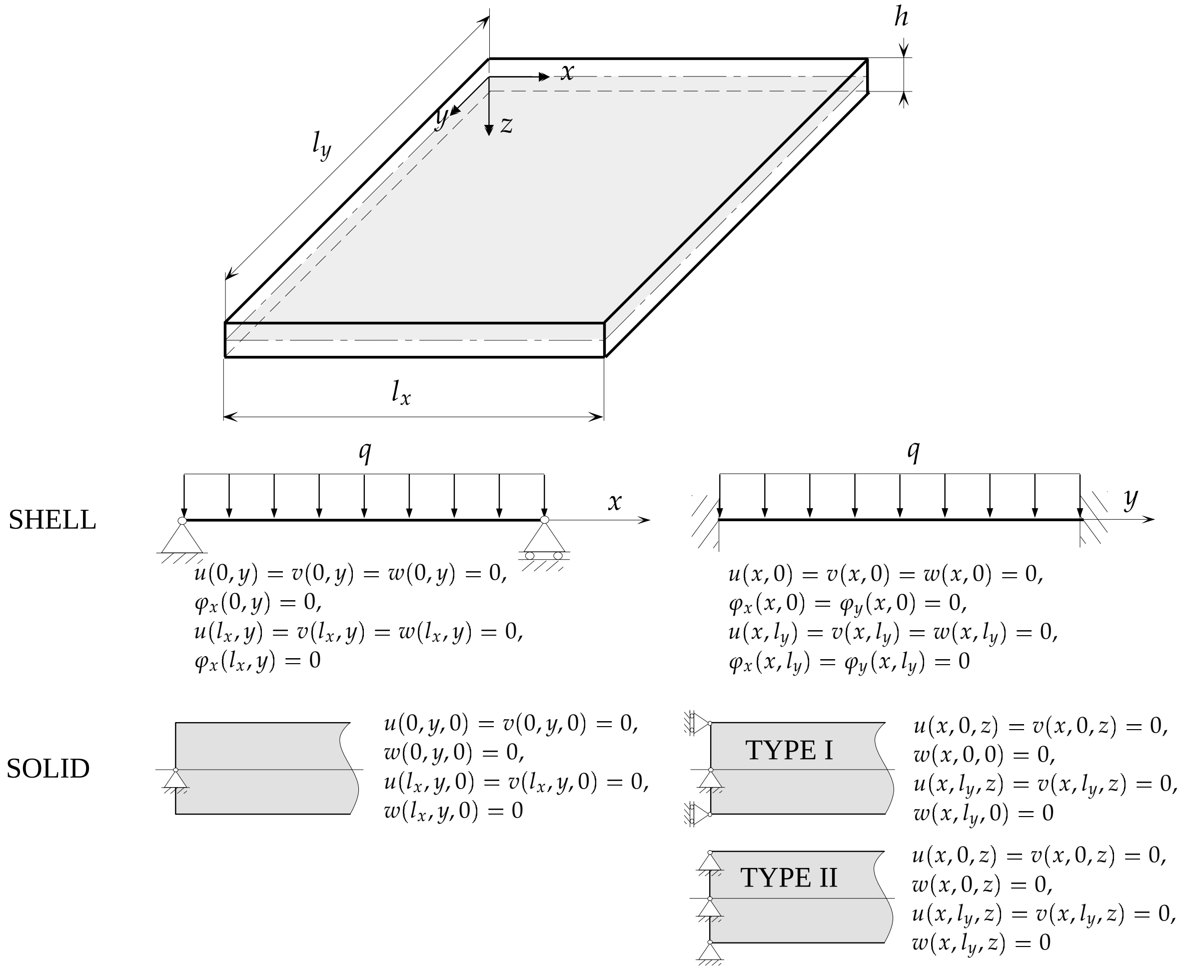

Figure 7: Rectangular plate: geometry and boundary conditions

and $x = l_x$ are simply supported and the edges $y = 0$ and $y = l_y$ are clamped. The analysis has been performed using the ANSYS finite element code after incorporating the material model (1) with the help of the user defined creep material subroutine. In [21] we discussed various examples for beams and plates in bending, which verify the modified subroutine. Two types of finite elements available in the ANSYS code for plasticity and creep analysis were used: the 20 nodes solid element SOLID 95 and the 4 nodes shell element SHELL 43 [22]. 30×15 elements were used for a half of the plate in the case of the shell model and $30 \times 15 \times 3$ elements in the case of the solid model. The meshes have been justified based on the elasticity solutions and the steady state creep solutions neglecting damage. With these meshes the reference stress distributions as well as distributions of the von Mises stresses in the steady creep state were approximately the same for both the solid and the shell elements and did not change by further re-meshing. For details of time integration and equilibrium iteration methods used in ANSYS for creep calculations we refer to [22] and [23]. The time step based calculations were performed up to $\omega = \omega_* = 0.9$, where ω_* is the critical value of the damage parameter.

According to the Reissner-Mindlin type plate (shell) elements [22] we can prescribe kinematical boundary conditions in terms of three displacements u, v, w of the plate middle surface (u and v denote the in-plane displacements and w is the deflection) and two rotations φ_1 and φ_2. In the case of the 3-dimensional model three displacements can be prescribed on the plate edges in all nodes of the thickness direction. Fig. 7 illustrates the used kinematical boundary conditions for the shell and the solid models. Let us note that the boundary condition of the clamped edge can be realised by different ways applying the solid model. In order to demonstrate the influence of boundary layers on creep solutions two types of boundary conditions corresponding to the model of clamped edge are introduced. In the first type (TYPE I), see Fig. 7, we assume the in-plane displacements u and v to be restricted in all nodes across the thickness direction. The deflection w is zero in the nodes of the plate middle surface only. In the second type (TYPE II) all three displacements are assumed to be zero in all nodes across the thickness direction. The difference between these two types of the boundary conditions can be simply established based on the governing equations of elasticity theory. For example if we consider the completely clamped edge $y = 0$ then we can assume $\varepsilon_x = \varepsilon_z = 0$ in all points of the edge. From the generalised Hooke's law

$$\sigma_{ij} = \frac{E}{1+\nu}\left(\varepsilon_{ij} + \frac{\nu}{1-2\nu}\delta_{ij}\varepsilon_{kk}\right)$$

we obtain according to the boundary conditions

$$\sigma_x = \sigma_{11} = \frac{E}{1+\nu}\frac{\nu}{1-2\nu}\varepsilon_y, \ \sigma_y = \sigma_{22} = \frac{E}{1+\nu}\frac{1-\nu}{1-2\nu}\varepsilon_y, \ \sigma_z = \sigma_{33} = \frac{E}{1+\nu}\frac{\nu}{1-2\nu}\varepsilon_y$$

Frome the above equations follows

$$\sigma_x = \sigma_z = \frac{\nu}{1-\nu}\sigma_y$$

With $\nu = 0.314$ for the considered 316 stainless steel we obtain for the transverse normal stress $\sigma_z \approx 0.458\sigma_x$. The assumed completely clamped edge conditions correspond are the boundary conditions of the TYPE II, Fig. 7. In the case of the TYPE I we can observe that $\sigma_z = -q$ on the plate top surface and $\sigma_z = 0$ on the plate bottom surface. The TYPE I of the boundary conditions corresponds to the assumptions of the Reissner type plate theory (in the case of beam see Section 3). Therefore the elasticity solutions obtained from the finite element simulation according to the SOLID model with TYPE I boundary conditions are in agreement with those obtained based on the SHELL model, Figs 8 and 9 (dotted lines). In the case of the SOLID model with TYPE II boundary conditions the boundary layer is observed for the transverse normal stresses σ_z, Fig. 9. The maximum transverse normal stresses are observable in the clamped edges and their computed values agree with the above estimate $\sigma_z \approx 0.458\sigma_x$. These maximum stresses decay

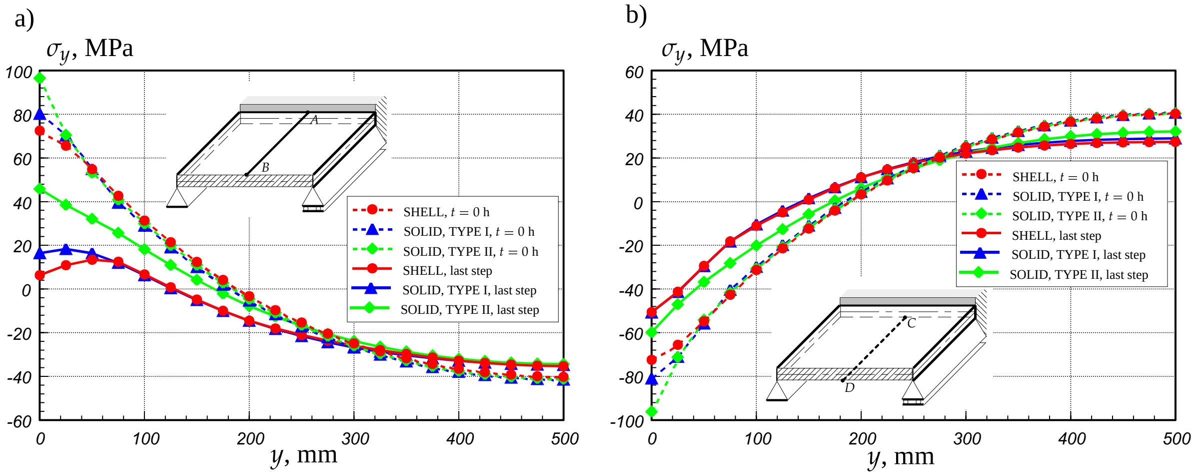

Figure 8: Distributions of bending stresses σ_y: (a) along the line AB, top surface; (b) along the line CD, bottom surface

rapidly with increased distance from the boundary and arrive to the values equal the given transverse load on the top surface and zero on the bottom surface. The distributions of σ_z for the solid model with TYPE I boundary conditions are the same as those obtained by use the plate theory. The solid lines in Figs 8 and 9 present the stress distributions obtained at the last time step of the creep process (critical damage state). It can be observed that the creep process significantly influences the distribution of bending stresses. The increase of the creep strains is accompanied by the relaxation of the bending stresses, Fig. 8. In contrast the distributions of transverse normal stresses do not change for the first two models or slightly change in the case of the solid model with TYPE II boundary conditions, Fig. 9. Because the stiffness of the plate with respect to the thickness changes is much higher as the bending stiffness we can assume that the transverse normal stresses are completely defined by the equilibrium conditions (statically determinate) and are not influenced by the creep strains. The results based on the shell elements agree again well with the results obtained with the solid mesh with TYPE I boundary conditions, Fig. 9. The difference between the obtained solutions based on three discussed models of the plate is clearly seen on the time variations of the maximum deflection and the maximum damage parameter, Fig. 10. In the example considered the shell model is conservative with regard to the life-time prediction, it overestimates the time to fracture and underestimates the maximum deflection. The solid model with the TYPE I boundary conditions yields shorter time to fracture and higher rate of the deflection growth. Similar effects were observed in Fig. 4a) for the beam and plane stress based solutions. Since the clamped edge boundary conditions of the TYPE I in the solid model correspond to those in the shell model one can explain the obtained differences to be the result of the constant shear correction factor and fixed (time independent) transverse shear stress distributions in the shell elements. The contributions of the transverse shear stress are discussed in detail in Section 3 for a beam. Fig. 12 shows the damage distribution obtained by use the solid model with TYPE II boundary conditions. The zone of the maximum damage is observable at the midpoint of the clamped edge on the top surface of the plate. The same zone

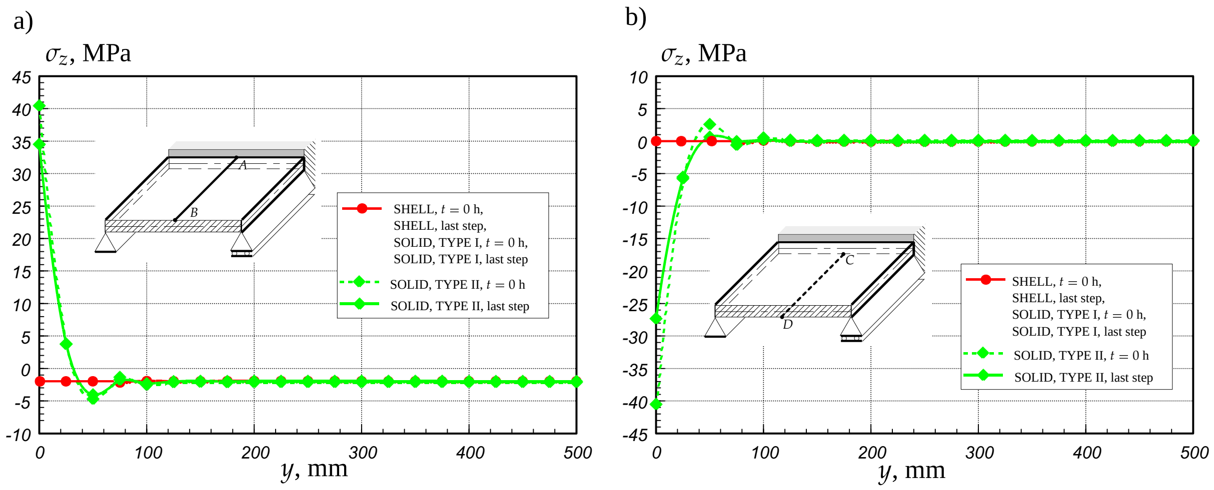

Figure 9: Distributions of transverse normal stresses σ_z: (a) along the line AB, top surface; (b) along the line CD, bottom surface

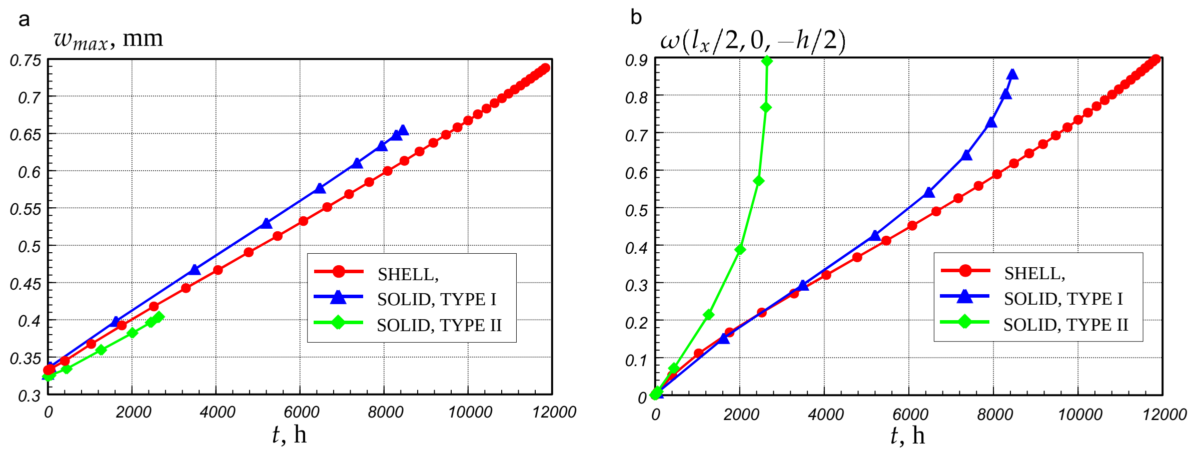

Figure 10: Time variations: (a) maximum deflection; (b) damage parameter

of the maximum damage is obtained if we apply the shell model or the solid model with TYPE I boundary conditions. However, the failure time predictions significantly differ for the three models applied. Fig. 12 illustrates the time variations of the three principal stresses in the Gauss point where the critical damage is obtained. The first principal stress σ_I is approximately equal the dominating bending stress σ_y, σ_{II} is determined by the bending stress σ_x and σ_{III} – by the transverse normal stress σ_z since the shear stresses are small in the point considered. Applying the solid model with TYPE I boundary conditions the third principal stress is approximately zero during the whole creep process, Fig. 12a). Therefore both the creep and the damage rates are controlled by the biaxial stress state determined by the two principal stresses. The same result is obtained using the model with shell elements. In contrast the boundary layer solution for σ_z resulting from the solid model with TYPE II boundary conditions is responsible to the

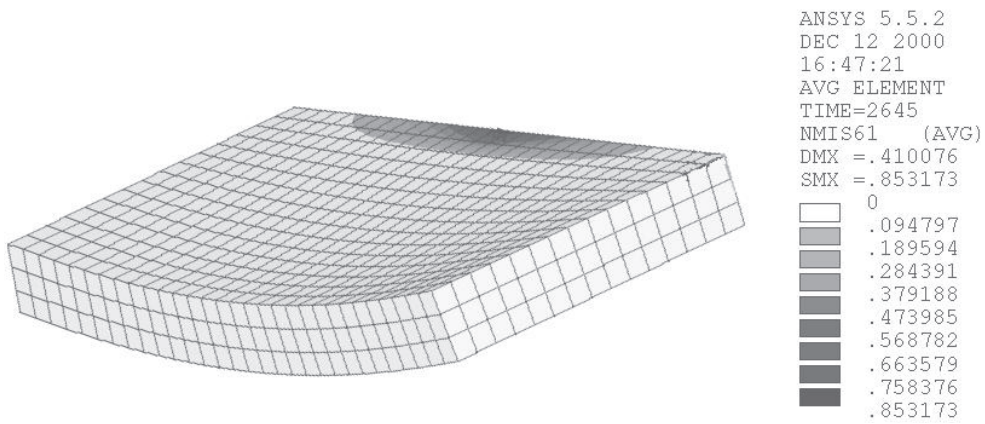

Figure 11: Damage distribution at last time step

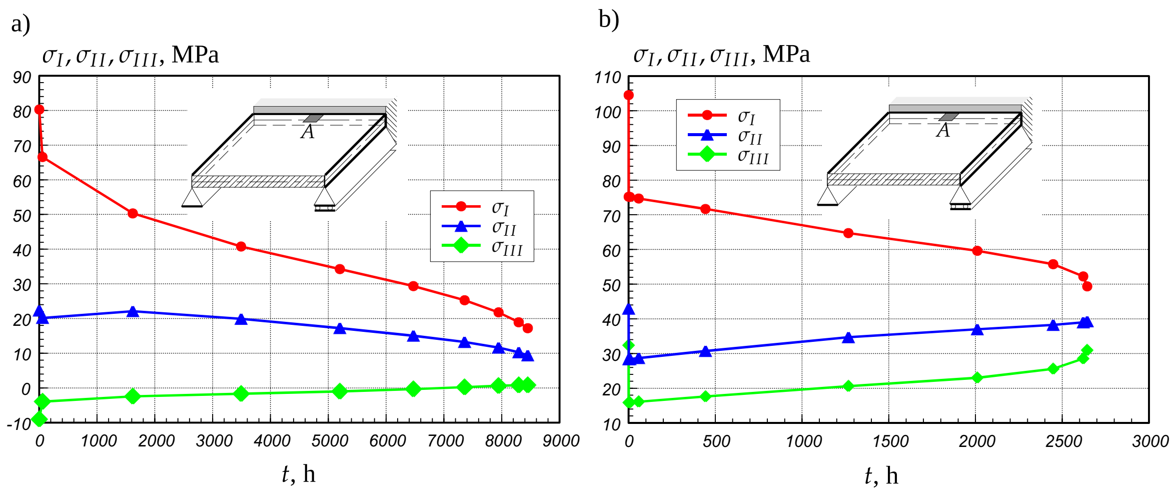

Figure 12: Principal stresses vs. time at point A: (a) SOLID, TYPE I; (b) SOLID, TYPE II

third principal stress, Fig. 12b). At $t = 0$ its value is much smaller then the value of the first principal stress. However, since the bending stress σ_y significantly relaxes as a consequence of creep and the transverse normal stress remains approximately constant we observe that the creep process is controlled by the triaxial stress state. Furthermore, with the stress relaxation the values of the three principal stresses become of the same order. As we discussed before, see Fig. 2, if all principal stresses tend to be equal, the triaxial stress state results in significant decrease of the creep strain rate. The damage rate remains the same since it is determined by the first principal stress only. Consequently, comparing the three models of the considered plate (the two-dimensional model and the solid models with different boundary conditions) we observe that in the case of TYPE II boundary conditions the deflection rate is smaller, see Fig. 10a), but the damage rate is much higher, see Fig. 10b).

5 Conclusions

We discussed non-linear time-dependent solutions based on the first order shear deformation equations of beams and plates as well as the corresponding three-dimensional models in connection with creep-damage material models. We demonstrated on the beam equations that the shear correction factor and the function of the thickness distribution of the transverse shear stress have to be modified by solving the creep-damage problems. This function is important for the correct estimation of the transverse shear stresses as well as of the averaged cross-section rotations and the averaged creep shear strain.

Further we performed the finite element analysis of a plate in bending with solid and shell type finite elements available in the ANSYS code. The results were compared for different types of boundary conditions corresponding to the model of a clamped edge. The disagreement between the results is observed on the edge zone stress redistributions. This is explained to be the result of the dependence of the creep response on the kind of the stress state induced by damage evolution. The transverse shear stress and the transverse normal stress can essentially influence the deformation behaviour if time-dependent creep and damage are taken into account. These stresses cannot be accurately computed within the framework of the first order shear deformation theory of beams, plates and shells.

Further investigations should be directed to the examinations of higher order terms in through-the-thickness displacement or stress field approximations of beams, plates and shells in connection with creep damage studies. The refined higher order theories should be discussed with respect to the accuracy of edge zone time-dependent stress redistributions for various types of boundary conditions.

Acknowledgement

The authors gratefully acknowledge the financial support from the German Research Foundation (DFG) under grant AL 341/15-1. Also, the authors acknowledge the support of the NATO Scientific Council for funding the research visit of Dr. V. Burlayenko.

References

[1] D. R. Hayhurst. The use of continuum damage mechanics in creep analysis for design. *J. of Strain Analysis*, **25**(3), 233–241, (1994).

[2] D. R. Hayhurst. Computational continuum damaged mechanics: its use in the prediction of creep in structures - past, present and future. In S. Murakami and N. Ohno, editors, *IUTAM Symposium on Creep in Structures*, pages 175–188, Dordrecht. Kluwer, (2001).

[3] E. Reissner. Reflections on the theory of elastic plates. *Appl. Mech. Rev.*, **38**(11), 1453–1464, (1985).

[4] H. Altenbach, J. Altenbach, and K. Naumenko. *Ebene Flächentragwerke*. Springer-Verlag, Berlin u.a., (1998).

[5] J. Betten, M. Borrmann, and T. Butters. Materialgleichungen zur Beschreibung des primären Kriechverhaltens innendruckbeanspruchter Zylinderschalen aus isotropem Werkstoff. *Ing. Arch.*, **60**(3), 99–109, (1989).

[6] N. Miyazaki. Creep buckling analyses of circular cylindrical shells under axial compression – bifurcation buckling analysis by the finite element method. *Trans. of ASME. J. Press. Ves. Techn.*, **109**, 179–183, (1987).

[7] S. Takezono and S. Fujoka. The creep of moderately thick shells of revolution under axisymmetrical load. In A. R. S. Ponter, editor, *Creep in Structures*, pages 128–143, Berlin et al. Springer-Verlag, (1981).

[8] A. Bodnar and M. Chrzanowski. Cracking of creeping plates in terms of continuum damage mechanics. *Mech. Teor. i Stos.*, **32**(1), 31–41, (1994).

[9] H. Altenbach, V. Kushnevsky, and K. Naumenko. On the use of solid and shell type finite elements in creep–damage predictions of thinwalled structures. *Arch. Appl. Mech.*, **71**, (2001). in press.

[10] K. Naumenko. On the use of the first order shear deformation models of beams, plates and shells in creep lifetime estimations. *Technische Mechanik*, **20**(3), 215–226, (2000).

[11] F. R. N. Nabarro and H. L. de Villiers. *The Physics of Creep. Creep and Creep–resistant Alloys*. Taylor & Francis, London, (1995).

[12] H. Riedel. *Fracture at High Temperatures*. Materials Research and Engineering. Springer, Berlin et al., (1987).

[13] I. J. Perrin and D. R. Hayhurst. Creep constitutive equations for a 0.5cr-0.5mo-0.25v ferritic steel in the temperature range 600-675°c. *J. of Strain Anal.*, **31**(4), 299–314, (1994).

[14] F. A. Leckie and D. R. Hayhurst. Constitutive equations for creep rupture. *Acta Metall.*, **25**, 1059 – 1070, (1977).

[15] Y. Liu, S. Murakami, and Y. Kanagawa. Mesh–dependence and stress singularity in finite element analysis of creep crack growth by continuum damage mechanics approach. *Eur. J. Mech., A Solids*, **13**(3), 395–417, (1994).

[16] Z. L. Kowalewski. Creep rupture of copper under complex stress state at elevated temperature. In *Design and life assessment at high temperature*, pages 113 – 122. Mechanical Engineering Publ., London, (1996).

[17] M. Sakane and T. Hosokawa. Biaxial and triaxial creep testing of type 304 stainless steel at 923 k. In S. Murakami and N. Ohno, editors, *IUTAM Symposium on Creep in Structures*, pages 411–418, Dordrecht. Kluwer, (2001).

[18] J. N. Reddy, C. M. Wang, and K. H. Lee. Relationships between bending solutions of classical and shear deformation beam theories. *Int. J. Solids. Struct.*, **34**(26), 3373–3384, (1997).

[19] E. Reissner. A variational theorem in elasticity. *J. Math. Phys.*, **29**, 90–95, (1950).

[20] F. K. G. Odqvist and J. Hult. *Kriechfestigkeit metallischer Werkstoffe*. Springer, Berlin u.a., (1962).

[21] H. Altenbach, G. Kolarow, O. Morachkovsky, and K. Naumenko. On the accuracy of creep-damage predictions in thinwalled structures using the finite element method. *Comp. Mech.*, **25**, 87–98, (2000).

[22] ANSYS User's Manual Volume I – IV. *Swanson Analysis Systems, Inc.*, (1994).

[23] O. C. Zienkiewicz and R. L. Taylor. *The Finite Element Method*. McGraw–Hill, London et al., (1991).